PREPRINT
Final paper: IEEE Sensors Journal 21 (2021), 22899 - 22907, 10.1109/JSEN.2021.3105879

A Position Sensor with Novel Configuration of Linear Variable Differential Transformer

Mehran Mirzaei, *Member, IEEE*, Pavel Ripka, *Member, IEEE*, and Vaclav Grim, *Student Member, IEEE*

***Abstract*—This paper presents a position sensor based on a novel configuration of linear variable differential transformer. Design and optimization of the position sensor are presented using finite element method. The sensor has short air core coils and long magnetic armatures. The arrangement direction of the rectangular excitation coil and two antiserially connected rectangular pick up coils is perpendicular to the motion direction of the position sensor. The coils are located between two parallel silicon steel laminations as the armatures. The position sensor is optimized with compromise between minimization of nonlinearity error and maximum sensitivity. The main advantage of the proposed position sensor is the small ratio of coils dimensions to the working range. The position sensor is operated for the measurements and calculations at excitation frequencies, 500 Hz and 1000 Hz and 2000 Hz. The maximum nonlinearity error is less than 1.5% for theoretical analysis and it is less than 2% for the measurement results in ±90 mm position range.**

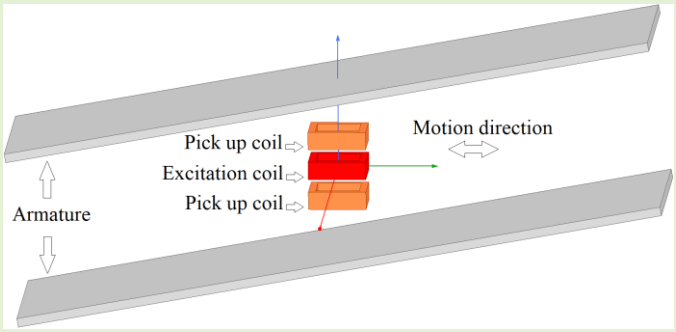

***Index Terms*—Position sensor, linear variable differential transformer, design and optimization, finite element method**

I. Introduction

THE position sensing and position sensors have a key role in various industrial applications and machineries with translational and rotational moving components [1]-[8]. The types of conventional position sensors are potentiometric, linear variable differential transformer (LVDT), optical, magnetostrictive, and magnetometer based, for example, magnetic Hall sensor.

Potentiometric position sensors have high accuracy, economical and simple signal processing [9]-[10]. However, they are sensitive to the wear, dust, and temperature. LVDT position sensors have high accuracy with lower sensitivity to the working environment [1] and [11]-[15]. They could be quite expensive and bulky because of the coils. Optical positions sensors are inflexible, sensitive to the dust and temperature despite their high accuracy and excellent resolution. Magnetometer based position sensors are sensitive to the magnetic objects and electrical noises, which affect their accuracy in position sensing [2] and [7]. Magnetostrictive position sensors [16] with high accuracy for long distance are sensitive to environment temperature, not cost effective and with less accuracy for short distance operation.

This work was supported in part by the Czech Technical University in Prague under Grant SGS18/187/OHK3/3T/1

M. Mirzaei is with Faculty of Electrical Engineering, Czech Technical University, Prague 16627, Czech Republic (e-mail: mirzameh@fel.cvut.cz).

P. Ripka is with Faculty of Electrical Engineering, Czech Technical University, Prague 16627, Czech Republic (e-mail: ripka@fel.cvut.cz).

V. Grim is with Faculty of Electrical Engineering, Czech Technical University, Prague 16627, Czech Republic (e-mail: vaclav.grim@fel.cvut.cz).

Position sensor based on variable inductance or impedance were presented in [17]-[19], which has bulky winding and heavy weight for long length measurements. Position sensors using magnetically coupled coils and short-circuited moving coil and air coil structure were designed and measured in [20]-[21]. However, these sensors suffer from low sensor output sensitivity and low immunity to the external adjacent magnetic objects. A variable reluctance differential solenoid transducer for position sensing was validated for high precision in [22], which is only shown for short lengths and it could be very bulky and heavy for large distance measuring. A permanent magnet linear resolver was used for position sensing for long distance in [23]. However, it needs salient secondary magnetic part with high precision punched or machine tooled and NdFeB permanent magnets with less appropriateness for harsh environments. Authors developed and presented long length position sensor for 500 mm working for pneumatic and hydraulic cylinders applications with small size coils and a conical solid iron rod [24].

A novel configuration of LVDT is utilized for position sensing in this paper with short coils and long armatures for long distance position measurements. The sensor can detect positive and negative movements as conventional LVDTs. The goal is to design a position sensor with highest simplicity for its structure and performance and to be cost effective. Armatures are only two silicon steel laminations with 0.5 mm thickness, which have been angularly shifted to the coils plane. Unlike the conventional LVDT sensor, the sizes of excitation and pick up coils are unchanged in this sensor to measure longer distance positions. 2D and 3D finite element method (FEM) is used for the performance analysis and design. The position sensor is designed and optimized to have high output sensitivity and low nonlinearity error.

II. Basic Study and Structure

Fig. 1 shows schematic 2D model of the position sensor, which consists of two armatures, one excitation coil and two antiserially connected pick up coils. The two armatures are in parallel and they are angularly shifted with angle, β relative to the coils in the horizontal plane (Fig. 1). Fig. 2 depicts schematic magnetic flux distributions at different relative positions of the coils and the armatures.

Equation (1) presents relationship between differential voltage, U_d and each pick up voltage, U_1 and U_2.

$$\begin{aligned} U_1 &= -j\omega \cdot \Psi_1 \\ U_2 &= -j\omega \cdot \Psi_2 \\ \omega &= 2\pi \cdot f \\ U_d &= U_2 - U_1 = -j\omega \cdot \Psi_d,\ \Psi_d = \Psi_2 - \Psi_1 \end{aligned} \quad (1)$$

Where, the differential flux linkage, Ψ_d is Ψ_2-Ψ_1, which Ψ_2 and Ψ_1 are flux linkage of pick up coils. f is the excitation frequency.

The upper and lower pick up coils have same flux linkage ($\Psi_2 = \Psi_1$) when they are located in the center position of armatures and their differential voltage is zero. However, the differential voltage value becomes negative or positive when the relative positions of the coils to the armatures are moved to the left or right directions. Because the flux linkages in pick up coil are different ($\Psi_2 \neq \Psi_1$) as distance between them and armatures are not the same as shown in Fig. 2.

3D model and dimensions of the position sensor are shown in Fig. 3. The number of turns in all coils is 500. The longitudinal length of armatures is 300 mm. The mean width, w_m and height, h of each coil are 11.6 mm and 5 mm as shown in Fig. 3. The position sensor performance is studied and measured at excitation frequencies, 500 Hz, 1000 Hz and 2000 Hz with corresponding measured current amplitudes, I_m, 84.7 mA, 83.0 mA and 79.4 mA, respectively.

III. FEM Study

2D and 3D time harmonic FEM [25] are used for the steady state performance analysis of the position sensor. The magnetic flux density is very low in the steel lamination of armatures as shown Fig. 4. Therefore, linear magnetic simulations are performed. And initial relative magnetic permeability, μ_r = 1000 for the steel lamination is estimated and considered for the FEM analysis [13] and [26]. The conductivity of steel lamination was measured, which is σ = 3.14 MS/m. The induced eddy current in the steel laminations is considered (Fig. 5) in the FEM analysis.

The following differential equations extracted from Maxwell equations are used in time harmonic magnetic field analysis:

$$\begin{aligned} \nabla \times H &= J \\ \nabla \bullet B = 0 &\rightarrow B = \nabla \times A \\ \nabla \times J &= -j\omega\sigma \cdot B \end{aligned} \quad (2)$$

where, H, J, B, and A are magnetic field strength, current density, magnetic flux density, and magnetic vector potential, respectively. Magnetic vector potential has only one unknown component, A_z in 2D analysis. But it has three unknowns, A_x, A_y and A_z. Therefore, 3D analysis is more time consuming and it needs more memory.

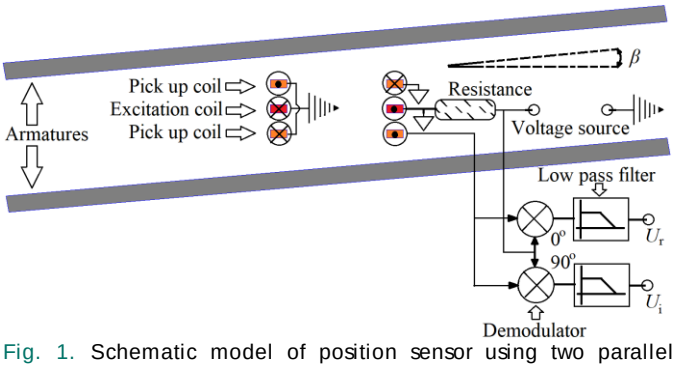

Fig. 1. Schematic model of position sensor using two parallel armatures with LVDT configuration and sensor measurement system using a lock in amplifier

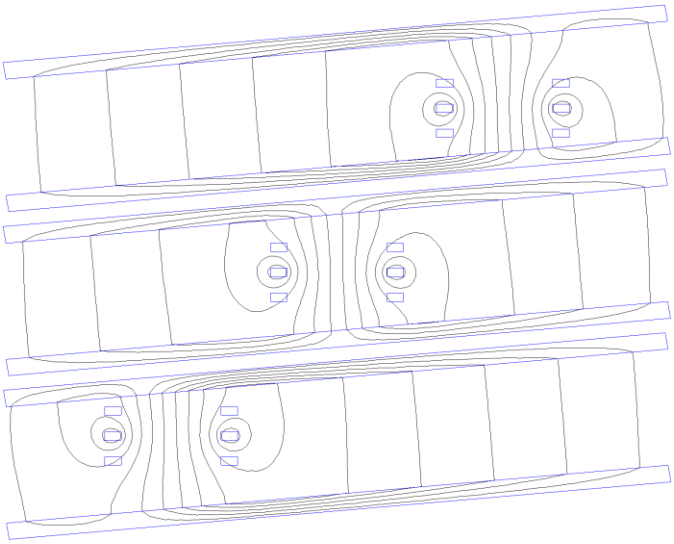

Fig. 2. Schematic magnetic flux distribution in the sensor at different relative positions of the coils relative to the armatures

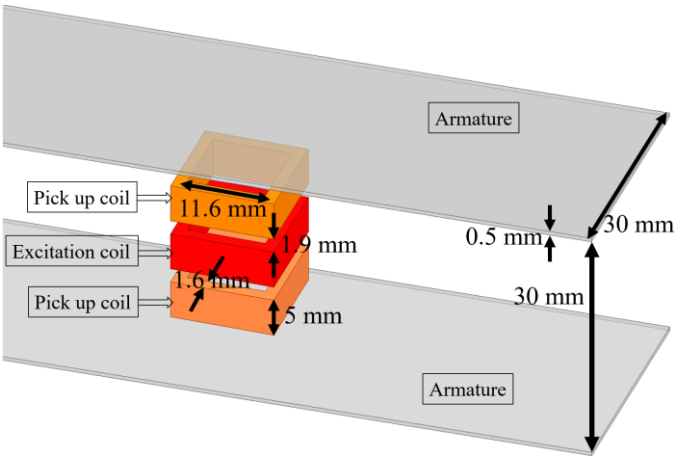

Fig. 3. 3D model of the position sensor and its dimensions

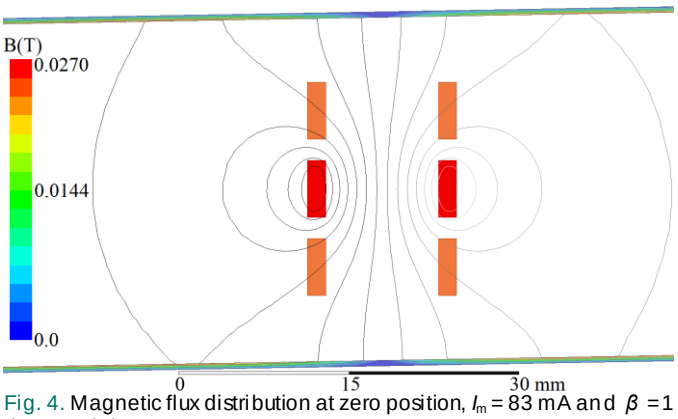

Fig. 4. Magnetic flux distribution at zero position, I_m = 83 mA and β =1 deg., and d = 0 mm – 2D FEM

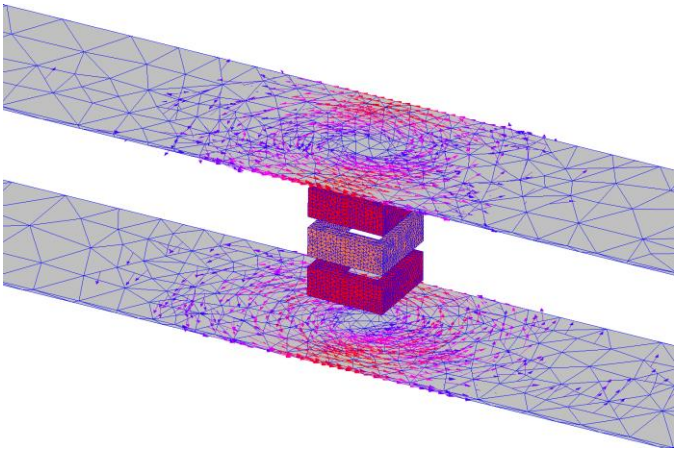

Fig. 5. 3D FEM meshed model of position sensor and induced eddy current in conductive silicon steel lamination with 0.5 mm thickness

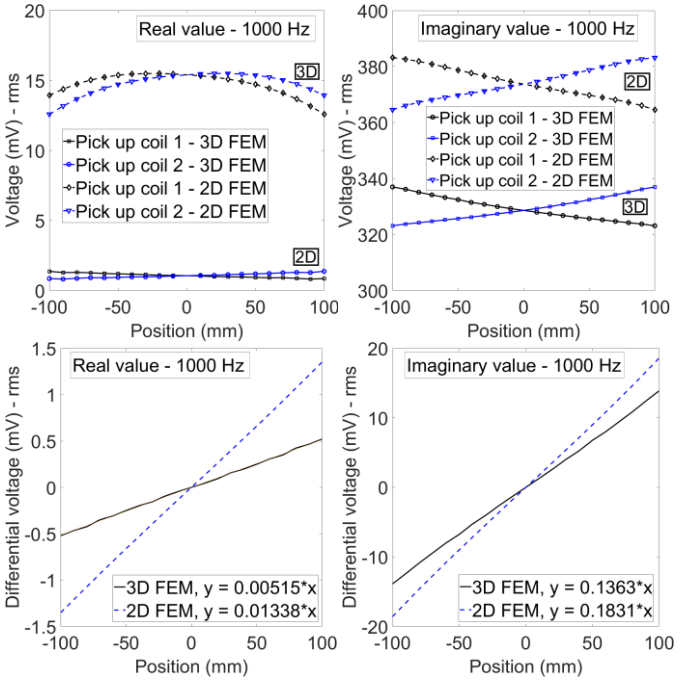

Fig. 6. The voltages of each pick up coils (U_1 and U_2) and their differential voltage (U_2-U_1) at 1000 Hz, I_m = 83 mA and β = 1.0 deg. – 2D FEM vs 3D FEM

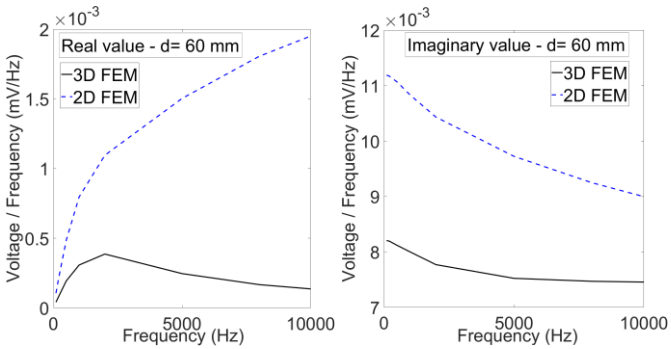

Fig. 7. The differential voltages normalized by frequency versus frequency, I_m = 83 mA, β =1 deg., and d= 60 mm – 2D FEM vs 3D FEM

The FEM analyses of the position sensor are performed in ±100 mm range. Fig. 6 shows the voltages of each pick up coil and their differential voltage versus position with β=1 deg. Real and imaginary components of voltages are calculated relative to the current of the excitation coil as a reference signal. Real component of voltage is caused by induced eddy currents in the conductive steel lamination of armatures. 3D FEM results shows less value in comparison with 2D FEM because of 3rd dimension effects (transverse effects), which is not considered in the 2D FEM. The model depth in transverse direction is considered 11.6 mm in 2D FEM, which is equal to the mean width of coil, w_c in Fig. 3. The differential voltages show linear curve versus positions in Fig. 6, which could be utilized as a position indicator.

The differential voltage to frequency ratio is depicted in Fig. 7 up to 10 kHz with β=1 deg., which is equivalent to differential flux linkage, Ψ_2-Ψ_1 in (1). It shows that the imaginary component of voltage is considerable higher than real component of voltage similar to the results in Fig. 6. The voltage to frequency ratio is decreasing with increasing frequency because of skin effects in the conductive steel laminations. Using nonconductive ferromagnetic armatures, for example, Ferrite will cancel frequency dependency of voltage to frequency ratio and diminish real component of voltage.

Absolute value of voltage, U_A can be also utilized for position sensing as both real, U_R and imaginary, U_I components are linear curve versus position.

$$U_A = \sqrt{U_R^2 + U_I^2} \tag{3}$$

Absolute value of voltage is almost as imaginary component of voltage as real component voltage is much smaller especially at operating frequency, 1000 Hz.

The differential voltages and nonlinearity full scale errors for different armatures shifting angles, β are presented in Fig. 8. The differential voltage is higher for bigger shifting angles, β. However, maximum nonlinearity full scale error is also increasing with bigger β. The calculated imaginary component of differential voltage has lower nonlinearity error, which makes it more suitable for position indicating at β = 0.5 deg. and 1.0 deg.

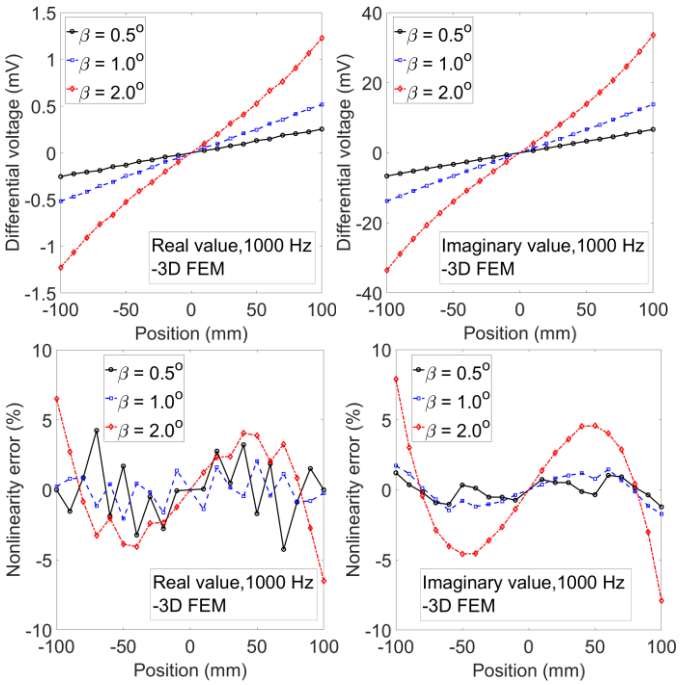

Fig. 8. The differential voltage and nonlinearity error at 1000 Hz, and I_m = 83 mA versus armatures angles, β

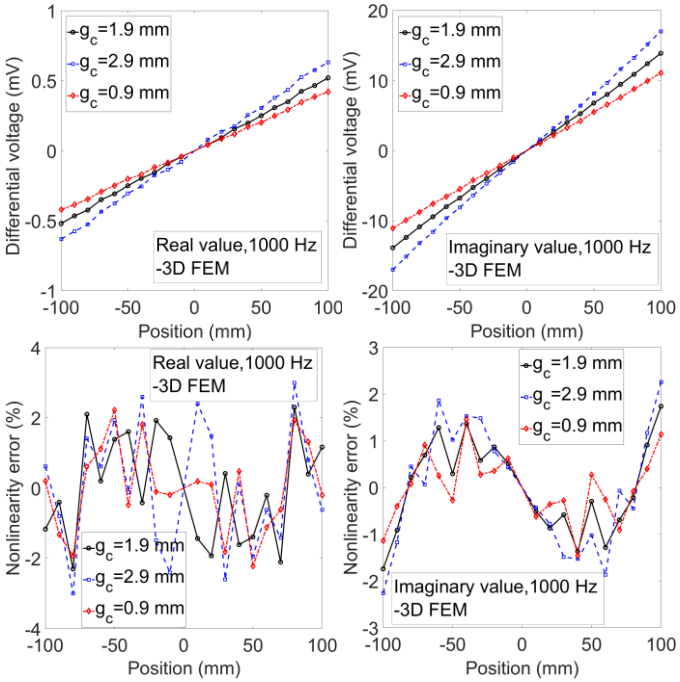

Fig. 9. The differential voltage and nonlinearity error at β = 1.0 deg., and I_m = 83 mA versus gap between excitation coil and pickup coils, g_c

Increasing gap distance between excitation coil and pick up coils, g_c increasing differential voltage with expense of increasing maximum nonlinearity full scale error as shown in Fig. 9. Selecting gap distance, g_c = 1.9 mm and armatures shifting angles, β=1.0 deg. is compromise between maximum differential voltage and minimizing of maximum nonlinearity full scale error.

Table I shows sensitivity coefficients, K_R and K_I of real and imaginary components of the differential voltage for different relative magnetic permeability, μ_r of silicon steel lamination of armatures. They are calculated based on linear curve fitting:

$$U_R = K_R \cdot X$$
$$U_I = K_I \cdot X \quad (4)$$

where, X is relative position of the coils and the armatures. Increasing or decreasing relative magnetic permeability, μ_r about 25% causes about 10% change in real component sensitivity, K_R and only 0.6% to 0.7% in imaginary component sensitivity, K_I.

TABLE I
SENSITIVITY FACTORS FOR DIFFERENT PERMEABILITY – 3D FEM

μ_r	K_R (mV/mm)	K_I (mV/mm)
750	0.005654 (109.7%)	0.1348 (99.3%)
1000	0.005154 (100.0%)	0.1358 (100.0%)
1250	0.004623 (89.7%)	0.1366 (100.6)

IV. EXPERIMENTAL RESULTS

The position sensors and experimental elements are shown in Fig. 10 and Fig. 11. Lock in amplifier is used for the voltage measurements of antiserially pick up coils. A signal generator with internal resistance 50 Ω is connected in series with excitation coil as source voltage. Also, an external 5.85 Ω resistance is connected in series with excitation coil and signal generator. It is utilized to measure the current of the excitation coil as a reference signal for the lock in amplifier, which real and imaginary components of pick coil voltage are finally measured relative to the reference signal. The schematic model of voltage measurement using lock in amplifier is also illustrated in Fig. 1. The reference position sensor in Fig. 11 is a potentiometer type.

Firstly, measured inductances of excitation coil and antiserially connected pick up coils and 3D time harmonic FEM calculations were evaluated with and without silicon steel laminations of armatures for the initial assessment of modeling. The results are presented in Table II and Table III at 500 Hz, 1000 Hz and 2000 Hz. The 3D FEM results match better with measurements for pick up coils inductances, L_{PK}, however, they are also in adequate range for excitation coil inductances, L_{EC}. The pick up coils inductances are more sensitive to armature position, d than excitation coil inductances.

TABLE II
COMPARISON BETWEEN EXPERIMENTAL AND 3D FEM – INDUCTANCES WITHOUT ARMATURES

	L_{EC} (mH)	L_{PK} (mH)
Exp.	3.470	6.2285
3D FEM	3.3279	6.2220

TABLE III
COMPARISON BETWEEN EXPERIMENTAL AND 3D FEM – INDUCTANCES WITH ARMATURES

	d= 0 mm	d= 0 mm	d= ±100 mm	d= ±100 mm
	L_{EC} (mH)	L_{PK} (mH)	L_{EC} (mH)	L_{PK} (mH)
f (Hz)	Exp./ 3D FEM	Exp./ 3D FEM	Exp./ 3D FEM	Exp./ 3D FEM
500	3.5190/ 3.3806	6.3910/ 6.3955	3.5195/ 3.3811	6.4170/ 6.4408
1000	3.5187/	6.390/	3.5187/	6.4158/

	3.3789	6.3934	3.3802	6.4383
2000	3.5169/	6.3878	3.5173/	6.4134
	3.3771	6.3890	3.3784	6.4333

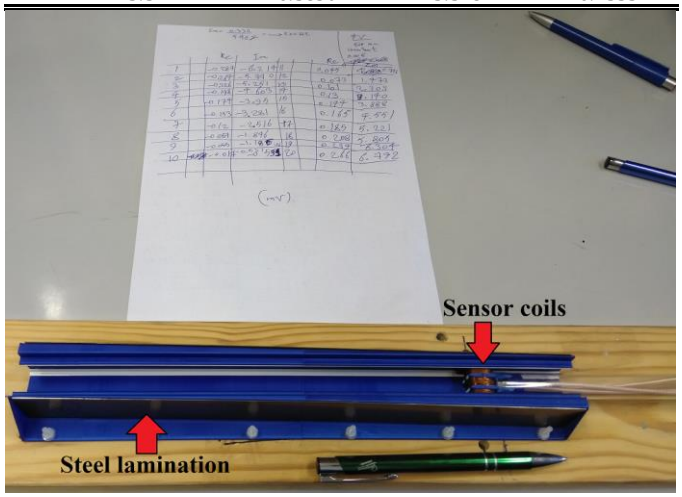

Fig. 10. The position sensor – Excitation coil, pickup coils and steel laminations

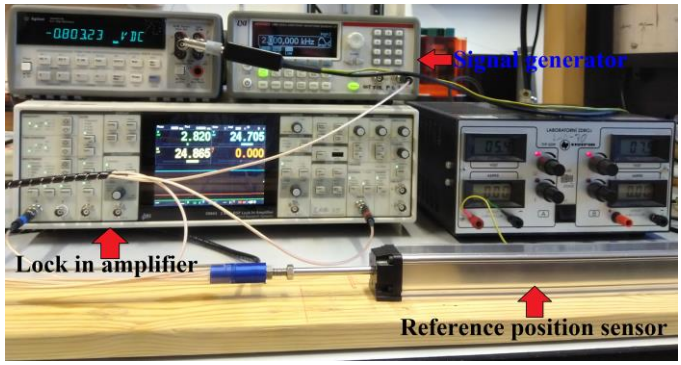

Fig. 11. Experimental elements – lock in amplifier, signal generator, and reference position sensor

The measured real and imaginary components of differential voltage and their full scale nonlinearity errors versus position are presented in Fig. 12 at 500 Hz, 1000 Hz and 2000 Hz. The measured real component of voltage curve is smaller and less linear in comparison with imaginary component. The imaginary component sensitivity is about 8.6 times higher than real component sensitivity at 2000 Hz and it increases up to 14.0 and 23.7 at 1000 Hz and 500 Hz, respectively.

The maximum nonlinearity error is close to the 5% for real component of voltage and it is less than 4% for imaginary component for ±100 mm operating range. However, the maximum nonlinearity error is less than 2% for ±90 mm operating range. The high nonlinearity error at ±100 mm for armatures position is mainly caused by manufacturing tolerance. As this high nonlinearity error is absent in 3D FEM at ±100 mm in Fig. 9. The full scale nonlinearity error is less than 1.5% for whole ±100 mm working range in 3D FEM results.

High nonlinearity error of real component of differential voltage has not considerable effect on the absolute value of differential voltage as shown in Fig. 13. The sensitivity coefficient of absolute value of differential voltage, K_A increases 0.7% in comparison with sensitivity coefficient of imaginary component at 2000 Hz and it increases 0.2% and 0.1% at 1000 Hz and 500 Hz, respectively.

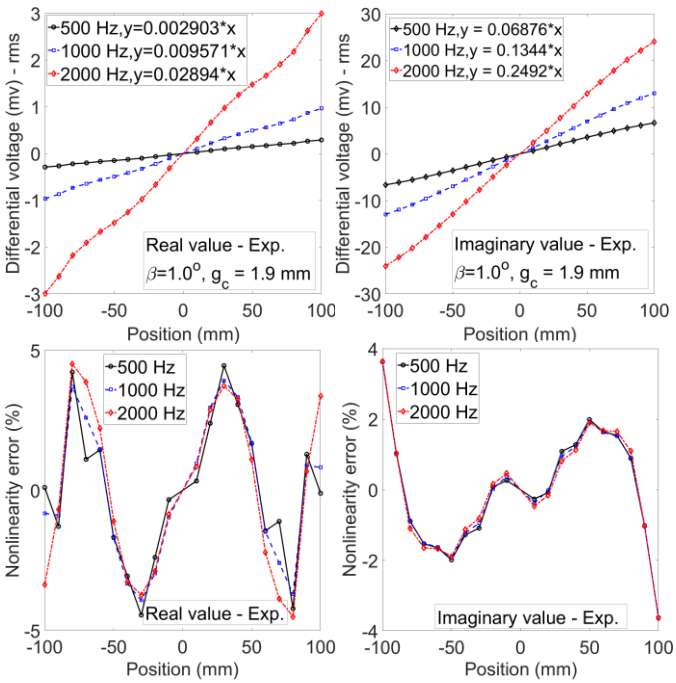

Fig. 12. The differential voltage and nonlinearity error – Experimental results for real and imaginary components

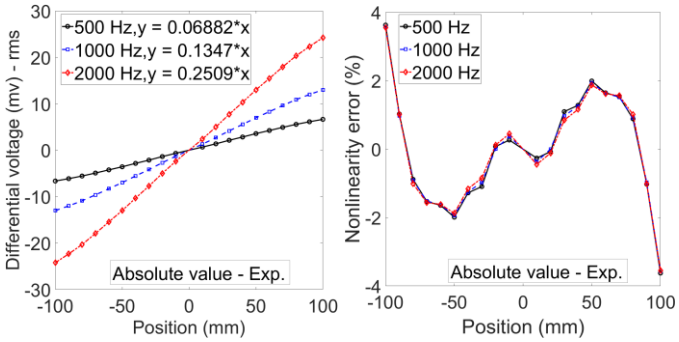

Fig. 13. The differential voltage and nonlinearity error – Experimental results for absolute value

V. Dynamic Analysis

The performance of the position sensors is important in dynamic conditions, especially, when the sensors have conductive components. The dynamic modeling using 2D time stepping FEM analysis of the position sensor at variable speeds are performed to evaluate motional induced eddy current effects on the sensor performance. The motional induced eddy current is generated when solid conducting armatures have relative speed to the excitation coil [27]-[29]. 2D time stepping FEM is used for the dynamic analysis despite its lower accuracy. Because it has less limitation in terms of number of meshes and memory, which is not straightforwardly conceivable in 3D time stepping FEM [30].

Two different speed profiles, 1 and 2 are selected for dynamic analysis for time range 100 ms as shown in Fig. 14. The positions of armatures, d versus time change from -60 mm

to +15 mm in both speed profiles, but they have different curves. The differential voltages versus armatures position are shown for speed profiles, 1 and 2 in Fig. 15 at 500 Hz and 1000 Hz, which are the same for two speed profiles. It can be confidently mentioned that motional component of induced eddy current in steel laminations has negligible effects on the performance of the position sensor.

VI. Discussions

Using ratiometric function $((U_2\text{-}U_1)/(U_2+U_1))$ reduces sensitivity of the position sensor to the armature material parameters, frequency and current of the excitation coil [11]. For example, Table IV shows sensitivity coefficients using ratiometric function ($K_{R\text{-}r}$ and $K_{I\text{-}r}$) for relative magnetic permeability change, which shows maximum 3% change for real component sensitivity, $K_{R\text{-}r}$ and 0.4% to 0.6% in imaginary component sensitivity, $K_{I\text{-}r}$. It is less sensitive to the relative magnetic permeability change in comparison with sensitivity coefficient in Table I. Therefore, ratiometric function could be also utilized to compensate material effects and temperature effects on the performance of the position sensor.

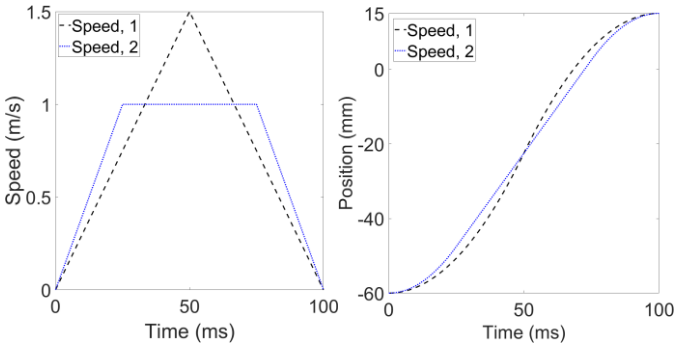

Fig. 14. Two applied time varying speed profiles

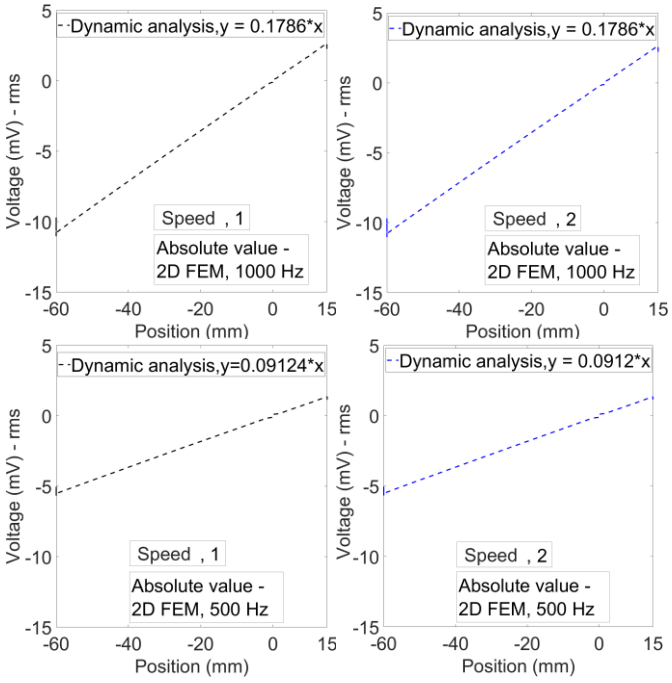

Fig. 15. The differential voltage versus position in dynamic conditions– 2D FEM

TABLE IV
Sensitivity Factors of Ratiometric Function for Different Permeability – 3D FEM

μ_r	$K_{R\text{-}r}$ (1/mm)	$K_{I\text{-}r}$ (1/mm)
750	0.002460 (103.0%)	0.0002048 (99.4%)
1000	0.002388 (100.0%)	0.0002060 (100.0%)
1250	0.002368 (99.2%)	0.0002069 (100.4)

Real and imaginary components of differential voltage versus frequency are measured and their ratio to frequency are shown in Fig. 16 at armature position, d= ±60 mm. The imaginary component is close to the 3D FEM simulations in Fig. 7, however, real component is closer to the 2D FEM.

Fig. 17 presents comparison between 3D FEM and experimental results for real and imaginary components of differential voltage versus position. The real component has higher discrepancy between measurements and 3D FEM, which is similar to the results comparison in Fig. 16. The highest discrepancy between experimental results and 3D FEM for imaginary component of differential voltage is occurred at 100 mm position of armature, which down bending of experimental curve causes high nonlinearity error as shown in Fig. 12 and Fig. 13.

Multi frequency electromagnetic method and compensation technique on phase signature could be also used to compensate the decentralization of coils and material effects in the position sensor [31]-[32] in addition to using ratiometric function [11]. Extension of linear range of the LVDT position sensors using techniques, for example, techniques based on the fractional order LVDT, LVDT inverse transfer characteristic and functional link artificial neural network allows sensor performance improvement for industrial applications [12], [14] and [33].

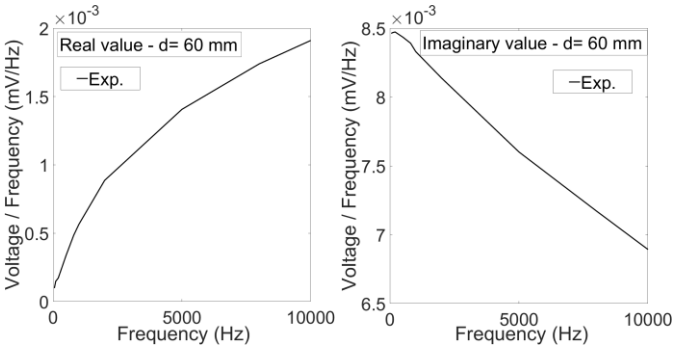

Fig. 16. The differential voltages normalized by frequency versus frequency, I_m = 83 mA, β =1 deg., and d= 60 mm – Experimental

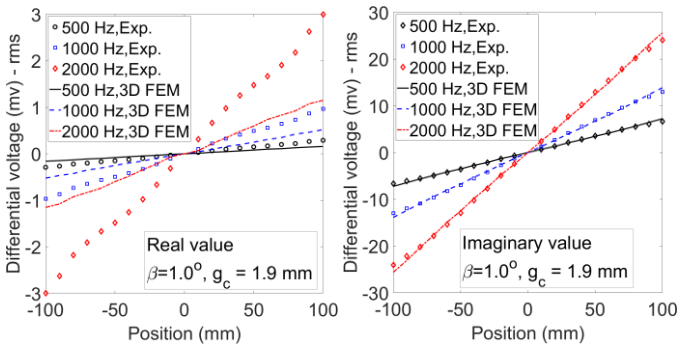

Fig. 17. The differential voltage– 3D FEM vs Experimental results

VII. Conclusion

The performance analysis and measurements of the position sensor with novel structure were presented. The sensor has simple configuration and it is cost effective, which makes it a suitable option for industrial applications and economically mass production. The small size of coils of the position sensor in comparison with armatures length and operating range makes it more fault tolerant in the harsh environment. And the position sensor is less bulky in comparison with its counterpart LVDT and potentiometer position sensors.

Conductive silicon laminations with 0.5 mm thickness were utilized for the armatures for easier manufacturing and lower material cost. However, it can be replaced with Ferrite, iron powder and soft magnetic composites rectangular bars with much lower conductivity to suppress induced eddy currents and minimize real component of differential voltage.

The measured sensitivities of the position sensor are 0.251 mV/mm, 0.135 mV/mm and 0.069 mV/mm for absolute value of differential voltage at 2000 Hz, 1000 Hz and 500 Hz, respectively. Maximum measured nonlinearity error is less than 2% in ±90 mm working range.

Optimization of the position sensor in terms of increasing sensitivity, reducing nonlinearity errors and extending linearity range is planned for the future works.

References

[1] C. W. Clapp, "Use of saturable cores in linear differential transformers," *IEEE Trans. Aerospace,* vol. 2, no. 4, pp. 1134-1142, Oct. 1964

[2] S. Taghvaeeyan, R. Rajamani, and Z. Sun, "Non-intrusive piston position measurement system using magnetic field measurements," *IEEE Sens. J.,* vol. 13, no. 8, pp. 3106-3114, Aug. 2013.

[3] M. Mirzaei, P. Ripka, A. Chirtsov, and V. Grim, "Temperature stability of the transformer position transducer for pneumatic cylinder," *J. Mag. & Mag. Mat.*, vol. 503, 166636, June 2020.

[4] P. Ripka, and A. Tipek, Modern Sensors Handbook. Chippenham, Wiltshire, UK: Wiley-ISTE, 2007, pp. 305-314

[5] X. Ge, Z. Q. Zhu, R. Ren, and J. T. Chen, "A novel variable reluctance resolver for HEV/EV applications," *IEEE Trans. Ind. App.*, vol. 52, no. 4, pp. 2872-2880, Jul./Aug. 2016.

[6] A. S. A. Kumar, B. George, and S. C. Mukhopadhyay, "Technologies and applications of angle sensors: a review," *IEEE Sens. J.,* vol. 21, no. 6, pp. 7195-7206, Mar. 2021.

[7] J. O. Manyala, T. Fritz, and M. Z. Atashbar, "Integration of triaxial Hall-Effect sensor technology for gear position sensing in commercial vehicle transmissions," *IEEE Trans. Inst. & Meas.*, vol. 61, no. 3, pp. 664-672 March 2012.

[8] J. Vcelak, Pavel Ripka, and Ales Zikmund, Long-range magnetic tracking system, *IEEE Sens. J.,* vol. 15, no. 1, pp. 491-496, Jan. 2015.

[9] Y. Kim, H. Y. Choi, and Y. C. Lee, "Design and preliminary evaluation of high-temperature position sensors for aerospace applications," *IEEE Sens. J.,* vol. 14, no. 11, pp. 4018-4025, Nov. 2014.

[10] Y. Kim, and H. Y. Choi, "A geometric design study of high-temperature position sensors," *IEEE Sens. J.,* vol. 16, no. 19, pp. 7065-7072, Oct. 2016.

[11] S. C. Saxena, and S. B. Lal Seksena, "A self-compensated smart LVDT transducer," *IEEE Trans. Ins. & Meas.*, vol. 38, no. 7, pp. 748-753, June 1989.

[12] W. Petchmaneelumka, W. Koodtalang, and V. Riewruja, "Simple technique for linear-range extension of linear variable differential transformer," *IEEE Sens. J.*, vol. 19, no. 13, pp. 5045-5051, Jul. 2019.

[13] M. Mirzaei, J. Machac, P. Ripka, A. Chirtsov, J. Vyhnanek, and V. Grim, "Design of a flat-type magnetic position sensor using a finite-difference method," *IET Sc., Meas. & Tech.*, vol. 14 no. 5, pp. 514-524, Jul. 2020.

[14] S. K. Mishra, G. Panda, and D. Prasad Das, "A novel method of extending the linearity range of linear variable differential transformer using artificial neural network," *IEEE Trans. Ins. & Meas.*, vol. 59, no. 4, pp. 947-953, April 2010

[15] G. Chen, B. Zhang, P. Liu, and H. Ding, "An adaptive analog circuit for LVDT's nanometer measurement without losing sensitivity and range," *IEEE Sens. J.*, vol. 15, no. 4, pp.2248-2254, April 2015.

[16] F. Seco, J. M. Martin, and A. R. Jimenez, "Improving the accuracy of magnetostrictive linear position sensors," *IEEE Trans. Inst. & Meas.*, vol. 58, no. 3, pp. 722-729, March 2009.

[17] H. Sumali, E. P. Bystrom, and G. W. Krutz, "A displacement sensor for nonmetallic hydraulic cylinders," *IEEE Sens. J.*, vol. 3, no. 6, pp. 818-826, Dec. 2003.

[18] E. G. Bakhoum, and M. H. M. Cheng, "High-sensitivity inductive pressure sensor," *IEEE Trans. Inst. & Meas.*, vol. 60, no. 8, pp. 2960-2966, Aug. 2011.

[19] S.-H. Yang, K. Hirata, T. Ota and Y. Kawase, "Impedance linearity of contactless magnetic-type position sensor", *IEEE Trans. Magn.*, vol. 53, no. 6, 8001204, Jun. 2017.

[20] K. R. Sandra, B. George, and V. Jagadeesh Kumar, "A nonintrusive magnetically coupled sensor for measuring liquid level," *IEEE Trans. Ins. & Meas.*, vol. 69, no. 10, pp. 7716-7724, Oct. 2020.

[21] A. Grima, M. Di Castro, A. Masi, and N. Sammut, "Design enhancements of an ironless inductive position sensor," *IEEE Trans. Ins. & Meas.*, vol. 69, no. 4, pp. 1362-1369, Apr. 2020.

[22] B. A. Reinholz, and R. J. Seethaler, "Design and validation of a variable reluctance differential solenoid transducer," *IEEE Sens. J.*, vol. 19, no. 23, pp. 11063-11071, Dec. 2019.

[23] L. Sun, J. Taylor, X. Guo, M. Cheng, and A. Emadi, "A linear position measurement scheme for long-distance and high-speed applications," *IEEE Trans. Ind. Elect.*, vol. 68, no. 5, pp. 4435-4447, My 2021.

[24] M. Mirzaei, P. Ripka, and V. Grim, "A novel position sensor with a conical iron core," *IEEE Trans. Inst. & Meas.*, vol. 69, no. 11, pp. 9178 - 9189, Nov. 2020.

[25] https://www.ansys.com/products/electronics/ansys-maxwell, Accessed on 06.04.2021

[26] E. Both, "The permeability of silicon-iron at very low flux densities," *Trans. American Inst. Elec. Eng., P. I: Comm. & Elect.*, vol. 72, no. 5, pp. 656 - 664, Nov. 1953.

[27] Z. Liu, A. R. Eastham, and G. E. Dawson, "Further studies on an improved finite element method for moving conductor eddy current problems," *IEEE Trans. Mag.*, vol. 30, no. 5, pp. 2984-2987, Sep. 1994

[28] N. Allen, D. Rodger, P. C. Coles, S. Street, and P. J. Leonard, "Towards increased speed computations in 3D moving eddy current finite element modelling," *IEEE Trans. Mag.*, vol. 31, no. 6, pp. 3524-3526, Nov. 1995

[29] M. Mirzaei, P. Ripka, A. Chirtsov, and J. Vyhnanek, "Eddy current linear speed sensor," *IEEE Trans. Mag.*, vol. 55, no. 1, 4000304, Jan. 2019

[30] D. Rodger, "Modelling movement in electrical machines," *IEEE Trans. Mag.*, 2021 (Early access).

[31] M. Lu, Y. Xie, W. Zhu, A. Peyton, and W. Yin, "Determination of the magnetic permeability, electrical conductivity, and thickness of Ferrite metallic plates using a multifrequency electromagnetic sensing system," *IEEE Trans. Ind. Inf.*, vol. 15, no. 7, pp. 4111-4119, July 2019.

[32] M. Lu, R. Huang, W. Yin, Q. Zhao, and A. Peyton, "Measurement of permeability for ferrous metallic plates using a novel lift-off compensation technique on phase signature," *IEEE Sens. J.*, vol. 19, no. 17, pp. 7440-7446, Sept. 2019.

[33] P. Veeraian, U. Gandhi, and U. Mangalanathan, "Fractional order linear variable differential transformer: design and analysis," *Int. J. Electron. & Commun. (AEÜ)*, vol. 79, pp. 141–150, 2017